Eur. Phys. J. E **19**, 171–183 (2006)
DOI: 10.1140/epje/e2006-00017-4

THE EUROPEAN PHYSICAL JOURNAL E

Effective temperature and jamming transition in dense, gently sheared granular assemblies

F.Q. Potiguar[1,2,a] and H.A. Makse[1]

[1] Levich Institute and Physics Department, City College of New York, New York, NY 10031, USA
[2] Universidade Federal do Ceará, Departamento de Física, Campus do Pici, 60455-760, Fortaleza, Ceará, Brazil

Received 8 November 2005
Published online 21 February 2006 –

Abstract. We present extensive computational results for the effective temperature, defined by the fluctuation-dissipation relation between the mean square displacement and the average displacement of grains, under the action of a weak, external perturbation, of a sheared, bi-disperse granular packing of compressible spheres. We study the dependence of this parameter on the shear rate and volume fractions, the type of particle and the observable in the fluctuation-dissipation relation. We find the same temperature for different tracer particles in the system. The temperature becomes independent on the shear rate for slow enough shear suggesting that it is the effective temperature of the jammed packing. However, we also show that the agreement of the effective temperature for different observables is only approximate, for very long times, suggesting that this defintion may not capture the full thermodynamics of the system. On the other hand, we find good agreement between the dynamical effective temperature and a compactivity calculated assuming that all jammed states are equiprobable. Therefore, this definition of temperature may capture an instance of the ergodic hypothesis for granular materials as proposed by theoretical formalisms for jamming. Finally, our simulations indicate that the average shear stress and apparent shear viscosity follow the usual relation with the shear rate for complex fluids. Our results show that the application of shear induces jamming in packings whose particles interact by tangential forces.

PACS. 45.70.-n Granular systems – 45.70.Vn Granular models of complex systems; traffic flow

1 Introduction

Granular materials are collections of macroscopic particles which interact, essentially, through inelastic collisions, repulsive contacts, and friction. This idea is simple and can be applied to a great variety of systems in nature, such as grains of sand, and assemblies of balls. Their importance is enormous to some industry segments, for example, the food industry [1].

Even though granular materials may sound simple, their physics is not. For reviews on general properties of such systems refer to the work by Jaeger and collaborators [2].

The complex properties of granular systems make the development of a general theory describing their behavior a difficult problem. A statistical mechanics approach was proposed by Edwards [3,4] to describe dense, slowly driven packings of rigid grains. The strong assumption of Edwards is that the microscopic configurations, called *blocked* or *jammed*, that the system visits during its evolution are equally probable. By this hypothesis, Edwards derived a whole thermodynamics-like formalism for powders.

Makse and Kurchan [5] showed, for system of driven, compressible grains, that the quantity:

$$X_{\rm E}^{-1} = \frac{\partial S}{\partial E}, \tag{1}$$

where S is the entropy of the powder and E, its energy, is the same, within error bars, as an effective temperature $T_{\rm eff}$ obtained dynamically, as proposed by Cugliandolo *et al.* [6]. The quantity $X_{\rm E}$ is the compactivity analogous to the compactivity of Edwards [3] where instead of using the energy E it is used the volume V of the powder. This effective temperature, $T_{\rm eff}$, is defined through the fluctuation-dissipation relation (FDR) between the mean square displacement (MSD) and average displacement (AD) of grains in z-direction under the action of a weak external force f:

$$\left\langle [z(t) - z(0)]^2 \right\rangle = 2T_{\rm eff} \frac{\langle z(t) - z(0) \rangle}{f}, \tag{2}$$

the brackets indicate an average over time and particles. This parameter is also called configurational temperature

[a] e-mail: potiguar@fisica.ufmg.br

for it controls the structural relaxation of a jammed system. This idea was studied in a variety of systems including glasses [6–10], models of powders [11] and foams [12].

The purpose of the present paper is to deeper investigate this result. We study the dependence of the configurational temperature with the external parameters (volume fraction and shear rate). We show that it does not depend on the shear rate (for slow enough motion) and the particular species of particle, a result that we believe characterizes the jamming, and provide initial evidence that the effective temperature is a proper thermodynamic variable to describe the system. We also discuss the dependence of $T_{\rm eff}$ on the observable used in the fluctuation-dissipation calculation. It has been recently shown that the effective temperature of dense granular matter can be measured experimentally in a Couette cylinder filled with spherical grains and slowly sheared [13]. These results together with the work performed by other groups provide indications that the thermodynamics approach to dense granular matter is possible.

We also analyze the role played by the granular temperature, as mesured by the average of kinetic energy. The results indicate that it is not a thermodynamical parameter for dense regimes due to its strong dependence on the external parameters. We also observe the behavior of others macroscopic parameters of the packings, such as the average shear stress and apparent shear viscosity. The first observable follows the usual Herschel-Bulkeley law. There seems to be a violation of this law for states in low densities where there is a frictional force between grains. Besides, the denser states develop a yield stress at low shear rates. These dense states are in the regime where the effective temperature is the relevant parameter. This implies the same correspondence already observed for glass-forming liquids [10]. The apparent shear viscosity displays the shear-thinning behavior of complex fluids, suggesting that powders may be treated as such fluids.

The organization of this work is as follows. In Section 2 we present details of the procedures employed in the simulations. In Section 3, the results for the diffusion coefficients, mobilities, defined by the MSD and AD, respectively, and effective temperatures are presented. Also in this section, we discuss the role of the granular temperature. The calculation of the effective temperature via configurational averages in presented in Section 4. The results of the average macroscopic quantities measured, shear stress and apparent shear viscosity, are shown in Section 5. Finally the conclusions are drawn in Section 6.

2 Simulation

We use Molecular Dynamics (also called Distinct Element Method (DEM) [14]) to model our system. It is a bidisperse assembly of 1000 spheres, half large, half small, with radii ratio of $R_{\rm S}/R_{\rm L} = 0.818$, which are initially randomly generated in a periodic cubic cell of size L.

The spheres interact via normal and tangential forces [15]. The first one is given by Hertz law, $F_{\rm n}$. The second force is Mindlin's no-slip solution for the contact,

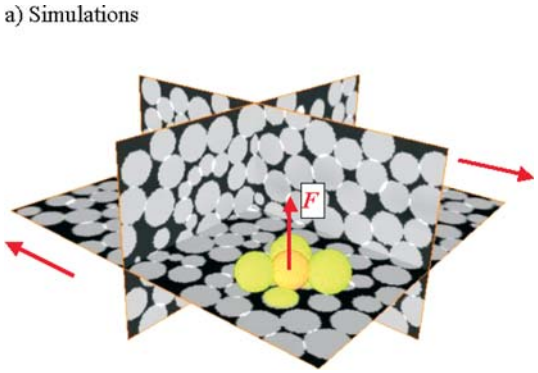

Fig. 1. Detail of the simulations of grains of 100 microns interacting via Hertz-Mindlin contact forces. A slow shear flow, indicated by the horizontal arrows, is applied to the jammed system. We follow the tracer particle trajectories to obtain the diffusivity. An external force F is then applied to the tracers in response to which we measure the particle mobility. These dynamical measurements yield an "effective temperature" obtained from an Einstein relation.

$F_{\rm t}$. The tangential force can increase up to the Coulomb threshold of friction $F_{\rm t} = \mu F_{\rm n}$ (where μ is the friction coefficient, typically $\mu = 0.3$). If $F_{\rm t}$ increases beyond $\mu F_{\rm n}$, the grains slide and the contact is broken. We also simulated packings in which particles interact only through normal forces, and we refer to these cases no friction, or frictionless, systems. We notice that the frictionless case would model a system of compressed emulsions [4,16]. Gravity is absent in all our simulations.

During the generation phase, no overlap between particles is allowed. We commonly have a initial volume fraction, ϕ, of the order of 0.25 in all our simulations. Since our goal is to study dense systems, we should compress the initial packing in order to attain a higher volume fraction. It is known [17] that there is a jamming transition at a critical volume fraction $\phi_{\rm c}$, corresponding to the random close packing (RCP). Above RCP there exists a mechanically stable solid-like state which is characterized by a non-vanishing internal stress and coordination number. Therefore, we choose three volume fractions, $\phi = 0.6428$, 0.6623, 0.7251, above RCP to perform our studies.

We study the jamming transition by performing simulations also below RCP, *i.e.*, in the fluid-like state. Such states can be prepared by expanding a previously equilibrated system above RCP to decrease the volume fraction up to the point where the pressure and the coordination number vanish, as reported in [17]. We prepare three fluid-like states with volume fractions given by $\phi = 0.5999$, 0.6104, 0.6318.

The simulations involve the application of shear in the x-y plane, at constant volume (see Fig. 1), with x the direction of the flow and y the velocity gradient. We follow the trajectory particles in the z-vorticity direction. We use a modified version of the usual Lees-Edwards boundary conditions [18] which imposes a linear velocity profile in the shear plane. Normal periodic boundary conditions are enforced in the z-direction. Segregation was not observed in the time scale of our runs.

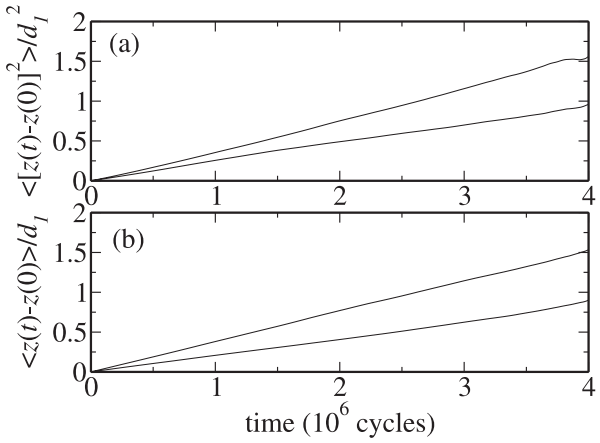

Fig. 2. (a) MSD and (b) AD for large (lower) and small (upper) particles in units of large particle diameter, d_1.

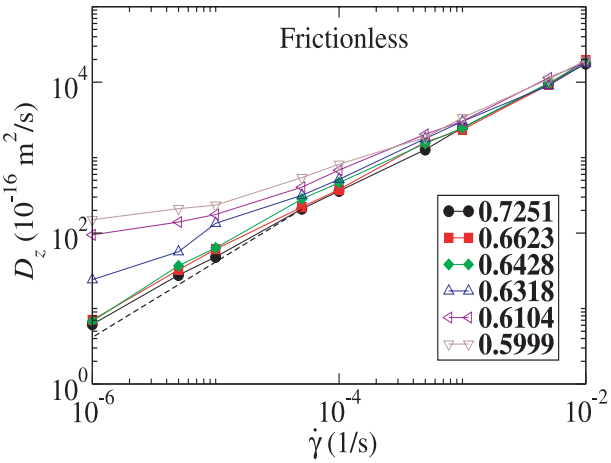

Fig. 3. Diffusion coefficient *vs.* shear rate, no friction.

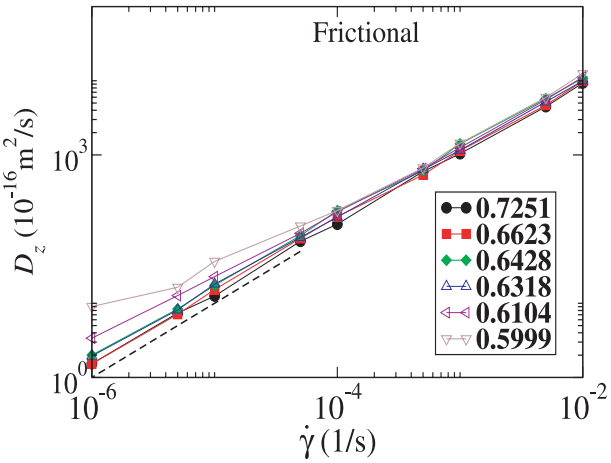

Fig. 4. Diffusion coefficient *vs.* shear rate, friction.

For each volume fraction, 9 different shear rates were considered, spanning a total of 5 decades of magnitude: $\dot{\gamma} = 10^{-6}, 5\times10^{-6}, 10^{-5}, 5\times10^{-5}, 10^{-4}, 5\times10^{-4}, 10^{-3}, 5\times10^{-3}, 10^{-2}\ \mathrm{s}^{-1}$. In our simulations time is given in seconds, length in meters, and mass in kilograms.

In what follows, we will calculate all the observables above and below RCP and for frictional and frictionless particles so that we will investigate the jamming transition at the RCP limit. The results shown in the next sections will be only for large particles, unless otherwise noticed. The results will be presented as functions of the shear rate, one curve for each volume fraction where applicable, in both frictional and frictionless cases. Moreover, since sheared systems enter a stationary state after an initial transient time [19,20] and does not display aging, it is sufficient to calculate all the following quantities as simple time averages. We calculate correlation and response functions with sets of overlapped data in the same run. We call this procedure window average. In practice it is the same as taking several time series in different runs and averaging over them. It saves run time and storage space.

3 Effective temperature

We calculate the effective temperature, T_{eff}, of the granular system by measuring it through equation (2), as in [5]. We investigate its dependence on the shear rate, and volume fraction. Next, we show that T_{eff} does not depend on the particular species on which it is being measured. Finally, we measure T_{eff} by a different FDT commonly used in the glass literature, the self-intermediate scattering function (ISF) and averaging over the jammed configurations.

3.1 Diffusion, mobility and FDT

The calculation of the diffusion coefficient in the z-direction, D_z, requires the evaluation of the MSD in this direction as a function of time:

$$2D_z t = \left\langle \frac{1}{N}\sum_{i=1}^{N}\left[z_i(t) - z_i(0)\right]^2 \right\rangle, \qquad (3)$$

where N is the number of particles considered, $z_i(t)$ is the z-coordinate of the ith particle at time t. The diffusion coefficient was calculated separately from the mobility (see below). In all plots, lines connecting the points are only guides to the eyes, unless otherwise noticed. Figure 2a shows the MSDs of the particles *versus* time from where the diffusion constant is extracted.

In Figures 3 and 4, we show the results for D_z for frictionless and frictional cases, respectively. First, we notice that the high volume fraction curves go to zero in a similar fashion, suggesting that our system is jammed [21]. Also, as the volume fraction decreases, particles have a higher diffusion for smaller shear rates. This is a consequence of the larger space available for particles to move under the influence of enduring contacts. As we go up in shear rate, this difference tends to disappear, the diffusion coefficient becomes independent on the density, due to the larger effect of inter-particle collisions.

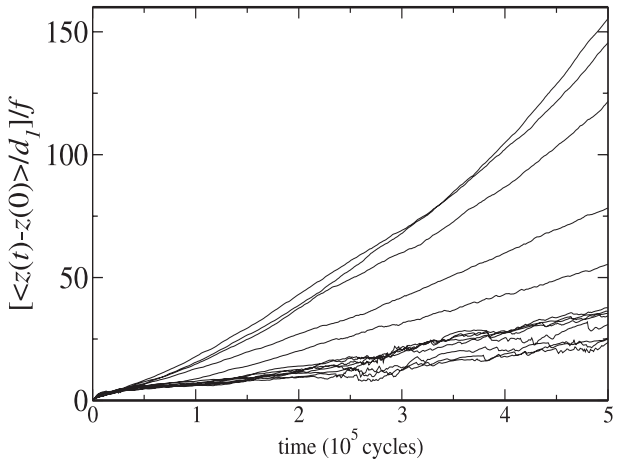

Fig. 5. Average z-displacement (given in units of large particle diameter) for force amplitudes of (from top to bottom) 0.06, 0.05, 0.04, 0.03, 0.02, 0.01, 0.009, 0.008, 0.007, 0.006, 0.005, 0.004, 0.003 N.

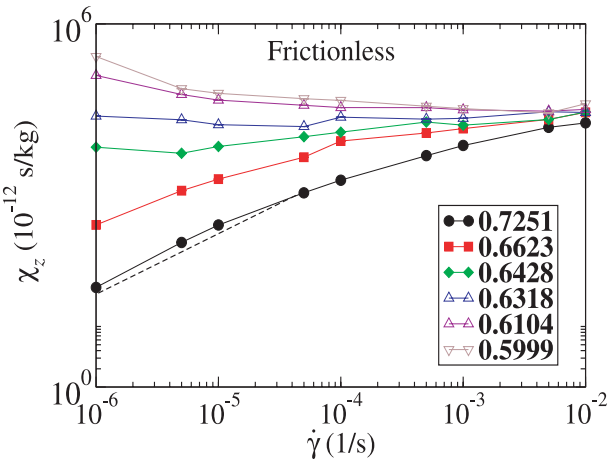

Fig. 6. Mobility *vs.* shear rate, no friction.

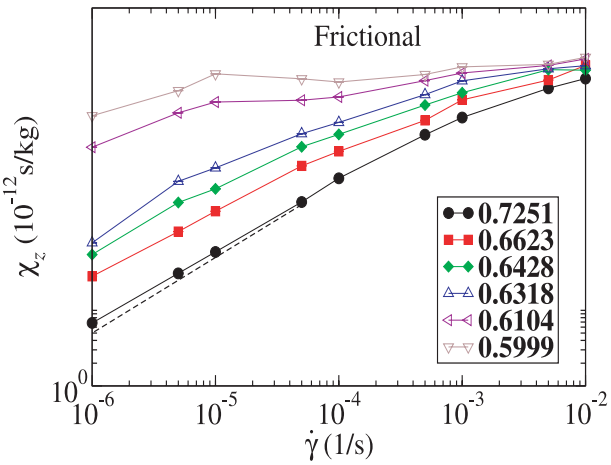

Fig. 7. Mobility *vs.* shear rate, friction.

In the case of friction, particles still diffuse more at lower densities than at higher densities but, somewhat surprisingly, the diffusion coefficient becomes independent on the density even for $\phi = 0.6318$, a fluid-like state. This is a first indication that the presence of friction between particles can induce the jamming transition for systems that are below RCP. This is usually called a shear-induced jamming transition, see [22,23].

The mobility, χ_z, is the response function associated with the motion of particles under an applied external force. To calculate χ_z, a small constant force is applied to each particle in order to induce a displacement in the z-direction. The mobility is taken as the slope of the curve of the average z-displacement, normalized by the applied external perturbation, *versus* time:

$$\chi_z t = \frac{1}{f}\left\langle \frac{1}{N}\sum_{i=1}^{N}\epsilon_i\left[z_i(t) - z_i(0)\right]\right\rangle, \qquad (4)$$

where f is the applied force, and $\epsilon_i = \pm 1$ is a "charge" set to each particle i. This is a standard procedure employed in numerical calculations to improve averages [24]. An average over a distribution of these charges yields the desired property.

Before calculating the mobility, we make short runs in each state considered for, at least, 10 forces in order to measure $\langle z(t) - z(0)\rangle / f$. The linear response regime is the range of forces where all z-displacement curves, normalized by the applied force, should overlap within numerical error. An example of this procedure is shown in Figure 5. Here, we show several displacement curves, for different applied forces, in the case of large, frictionless particles at volume fraction of $\phi = 0.6428$ and sheared at $\dot{\gamma} = 5 \times 10^{-6}$ s^{-1}. We can see clearly that for small forces all $\langle z(t) - z(0)\rangle / f$ curves are (without averaging) are within some well defined range, while at higher forces, the curves starts to deviate from the linear regime. After this regime is identified, we selected at least 5 values of the force to perform the calculation in longer runs.

Figures 6 and 7 show the results for χ_z for frictionless and frictional cases. Similarly to the case of diffusion, the mobility of the grains increases with decreasing volume fraction. Also, the presence of friction between grains diminishes the ability of particles to move, hence yielding a smaller mobility for these packings. The $\phi = 0.6318$ friction packing has similar dependence on $\dot{\gamma}$ as its denser counterparts, confirming the suspected shear-induced jamming transition indicated in the diffusivity plot of Figure 4.

A clear trend observed in the plots for D_z and χ_z is that, at lower volume fractions and shear rate, both D_z and χ_z have weaker dependence on shear rate, clearly observed in the no friction plots (and particularly, in the $\phi = 0.6428$ and $\phi = 0.6318$ cases). This fact indicates that these states are not jammed, since the ratio between D_z and χ_z, and consequently T_{eff}, would not be independent on $\dot{\gamma}$. A similar trend is displayed in the friction plot, but only to the two states at $\phi = 0.5999$ and $\phi = 0.6104$, and for shear rates above $\dot{\gamma} = 10^{-5}$ s^{-1}.

At higher volume fraction, we have a different picture. The dependence on the shear rate is approximately the same for all curves in all plots. This already suggests the

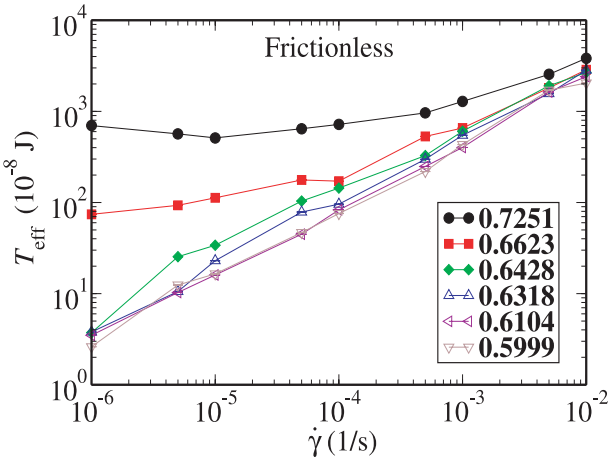

Fig. 8. Effective temperature *vs.* shear rate, no friction.

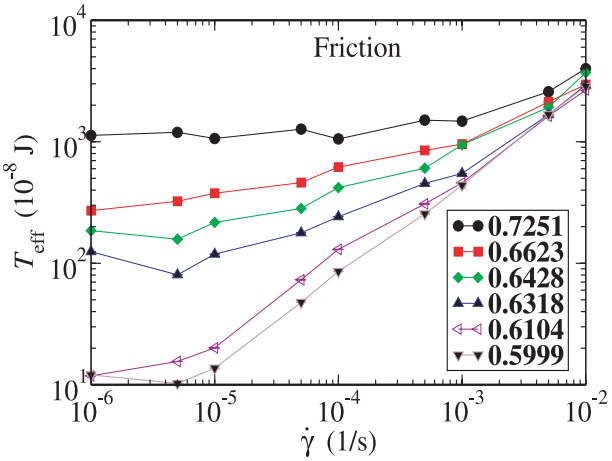

Fig. 9. Effective temperature *vs.* shear rate, friction.

regime where $T_{\rm eff}$ would be the relevant thermodynamical parameter. In these figures we put a dashed line with unity slope in order to indicate the expected behavior of both D_z and χ_z with the shear rate. We have close agreement in our results.

In Figure 2a we plot the MSD in the z-direction while in Figure 2b, the AD in z for large and small particles after the external force is applied. We find that the small tracer gives rise to a significantly larger diffusion constant than the large tracer. The same behavior is obtained for the mobility as can be seen in Figure 2b. This case was the $\phi = 0.7251$, frictionless one sheared at $\dot\gamma = 5 \times 10^{-6}$ s^{-1}. The perturbation was $f = 0.09$. All lengths are in units of large particle diameter, d_1. In Figure 2a, we measured $D_z/d_1^2 = 2.295 \times 10^{-7}$ s^{-1}, large, and $D_z/d_1^2 = 3.995 \times 10^{-7}$ s^{-1}, small particles. Figure 2b gave $\chi_z/d_1 = 2.232 \times 10^{-6}$ s/(kg m), large, and $\chi_z/d_1 = 3.741 \times 10^{-6}$ s/(kg m), small particles. The diffusion constant and the mobility are inversely related to the grain sizes. For a Stokes fluid we would expect that the ratios of the mobilities and diffusivities satisfy $D_{\rm s}/D_{\rm l} = d_{\rm l}/d_{\rm s}$, and $\chi_{\rm s}/\chi_{\rm l} = d_{\rm l}/d_{\rm s}$ where $d_{\rm s}$ and $d_{\rm l}$ are the diameter of the small and large particles respectively.

In our simulations, the ratio $d_{\rm l}/d_{\rm s}$ is equal to 1.22. We have, for example, the diffusion coefficients for the $\phi = 0.7251$ friction case, $\dot\gamma = 10^{-2}$ s^{-1}, are $D_{\rm l} = 9.317 \times 10^{-13}$ and $D_{\rm s} = 1.149 \times 10^{-12}$, their ratio yields 1.233, thus in good agreement with the Stokes result. Moreover, the mobilities for the state at $\phi = 0.6104$ volume fraction, sheared at $\dot\gamma = 5 \times 10^{-6}$ s^{-1} without friction have the values $\chi_{\rm l} = 6.818 \times 10^{-8}$ and $\chi_{\rm s} = 8.664 \times 10^{-8}$, whose ratio gives 1.27.

Now we pass on to the results of effective temperature. They are given in Figures 8 and 9. We can see that at higher volume fractions this effective temperature is approximately independent on the shear rate as $\dot\gamma \to 0$. This confirms what was stated before about the range of jammed states. Also, it is an important result for it shows that this is indeed an intrinsic property of the granular system, since it does not depend on the driving strength. The jammed state can be characterized by the independence of the effective temperature on the shear rate since this behavior is not observed in the other cases studied.

Two other conclusions may be drawn from these graphs. One is already expected from the previous plots: the state $\phi = 0.6318$ for the frictional case is indeed jammed, although it is below RCP. This confirms that the application of shear can induce a jamming transition in a friction packing. The second conclusion is that the state $\phi = 0.6428$ for frictionless particles is not jammed, even though it is above RCP. This indicates that frictionless particles are unstable under shear, however small.

Next, we test the zeroth law of thermodynamics for $T_{\rm eff}$. In other words, if the effective temperature has a physical thermodynamic meaning, it should be the same for different tracers in the medium. We test this by repeating the calculations of the MSD and the AD for both types of particles in frictionless states $\phi = 0.6428$ and $\phi = 0.6623$. Figure 10 shows the parametric plot of the two quantities at the cases considered, sheared at $\dot\gamma = 5 \times 10^{-6}$ s^{-1}. The agreement is clearly excellent. Although the curves for $\phi = 0.6428$ are in close agreement, the results for $T_{\rm eff}$ rules out the possibility that this state is jammed. This further suggests that $T_{\rm eff}$ is a good thermodynamic variable for the system.

3.2 Self-intermediate scattering function FDT

Another important characteristic of the effective temperature is that it should be independent of the particular observable (or fluctuation-dissipation relation) used in its measurement. In other words, we would like to know whether by measuring $T_{\rm eff}$ using different observables than those in equation (2) we obtain the same result. This independence on the observable was showed for supercooled liquids [10] and foams [12].

Here we use a quantity which was extensively studied in the glass literature, namely the self-intermediate scattering function (ISF) [8–10,25–27], defined as:

$$C_{k_z}(t) = \left\langle \frac{1}{N} \sum_{i=1}^{N} \exp\left\{ik_z\left[z_i(t) - z_i(0)\right]\right\} \right\rangle \qquad (5)$$

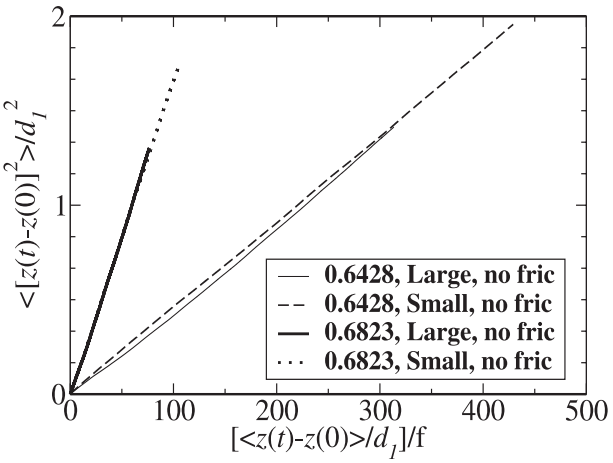

Fig. 10. Parametric plot of the MSD by AD. The legend displays the cases studied. All lengths are given in units of large particle diameters.

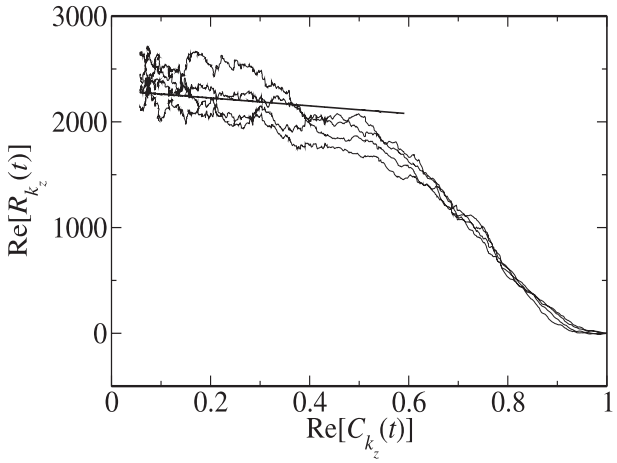

Fig. 11. The effective temperature (straight line) calculated from equation (2) overlaps with fluctuation-dissipation plots from equation (7) in the very long time limit. The amplitudes of the applied perturbations are (from top to bottom) 5×10^{-5}, 6×10^{-5}, 7×10^{-5}, and 8×10^{-5} N. This case is for frictionless particles, volume fraction of $\phi = 0.6428$ and shear rate of $\dot{\gamma} = 5\times10^{-6}$ s^{-1}.

where k_z is the wave vector in the z-direction. This function is the Fourier transform of the self part of the Van Hove correlation function at time t [24]. We chose the wave vector k_z as the peak of the static structure factor, which, in our case, is $k_z = 71.8L^{-1}$.

In order to measure a FDR (5) we apply a small force in each particle i of the form $F_i = -fk_z\epsilon_i \sin(k_z z_i)$, where f is the amplitude of the force. After the perturbation is applied we measure the response function, defined as:

$$R_{k_z}(t) = \frac{1}{f}\left\langle \frac{1}{N}\sum_{i=1}^{N}\epsilon_i \exp\left[ik_z z_i(t)\right]\right\rangle. \tag{6}$$

The amplitude f is the quantity which controls the intensity of the force. Therefore we set it to be small enough so that we measure R_{k_z} in the linear response regime. As in the mobility calculation, we search for the linear response regime by measuring the response function for several forces before performing the full calculation. Also, we did not employ the window average in the calculation of equation (6), instead we averaged over different measurements, 20, for each force.

The effective temperature is defined as the ratio between the real parts of equations (5) and (6):

$$T_{\text{eff}} = -\frac{\text{Re}\left[C_{k_z}(t)\right]}{\text{Re}\left[R_{k_z}(t)\right]}. \tag{7}$$

We measured this effective temperature for the $\phi = 0.6428$ frictionless state sheared at $\dot{\gamma} = 5\times10^{-6}$ s^{-1}. In order to test the equivalence of both temperatures, we plotted all results for equation (7) parametrically and a straight line with slope $-{T_{\text{eff}}}^{-1}$, with its value given by the corresponding result from equation (2). This is shown in Figure 11 for large particles. We see that the straight line has slope in the order of magnitude, only for very long times, as the one obtained from the ISF. Thus, it possibly indicates that T_{eff} do not capture all the statistical mechanics of the jammed state.

3.3 The role of kinetic energy

The kinetic energy is defined as the sum of the velocity fluctuations of all particles:

$$2E_{\text{K}} = \sum_{i=1}^{N} m_i \left(\mathbf{v}_i - \langle\mathbf{v}_i\rangle\right)^2, \tag{8}$$

where m_i is the ith particle's mass and $\mathbf{v}_i$, is the velocity vector.

As in thermal systems, we can define a parameter, called granular kinetic temperature, T_{K}, which is the average of equation (8) divided by $3N$. Since the average velocity is zero in the z direction, since there is no bias in this direction, we take T_{K} as the following expression:

$$T_{\text{K}} = \frac{1}{N}\sum_{i=1}^{N} m_i {v_z}^2. \tag{9}$$

This is an estimate of the temperature of the fast modes of the system [6,19] (since a granular system is athermal by definition). In thermal systems, equation (9) yields the bath temperature. It is expected, in the dense limit, that T_{K} does not share the same characteristics of T_{eff}.

In Figure 12, we show the kinetic temperature for both large and small particles for the highest and lowest volume fractions studied in the frictionless case. It is directly seen that such plots evidence the difference of T_{K} for both species of particles. We also notice that the kinetic temperature has two different regimes. One at high shear rate, where it is almost density independent. This is the fluid regime where the kinetic energy is dissipated at a smaller pace than in the dense case, this dissipation made mainly by collisions between grains. At low shear rates, the effect of volume fraction shows up. The denser the system,

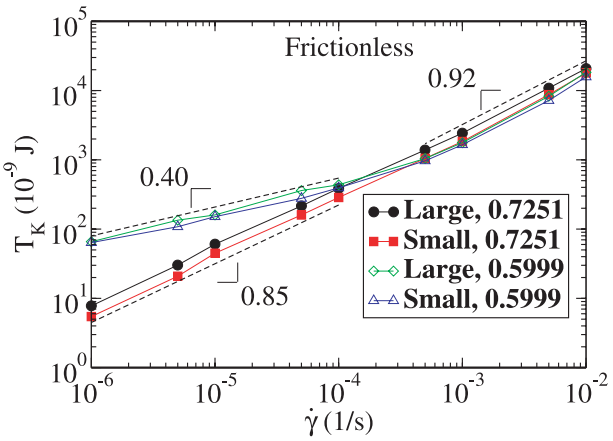

Fig. 12. Average kinetic temperature *vs.* shear rate, no friction, for large and small particles. The legend displays the cases showed. The dashed lines are fits to the curves and the numbers are the slopes of these lines (explained in the text).

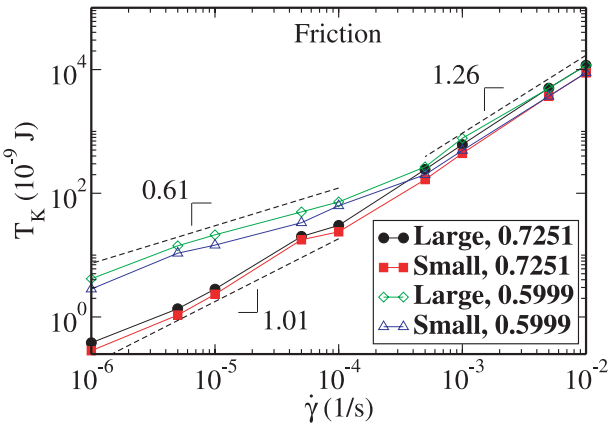

Fig. 13. Average kinetic temperature *vs.* shear rate, friction for large and small particles. The legend indicates the cases showed. The dashed lines are fits to the curves and the numbers are the slopes of the lines (explained in the text).

the smaller the kinetic temperature, as expected, since at high volume fractions there is a large number of contacts in the packing, which rapidly dissipate kinetic energy. In this case, the kinetic temperature depends on the shear rate again as a power law, but with a density dependent exponent.

Figure 13 shows the kinetic temperature for large and small particles, in the lowest and highest volume fractions considered here for frictional packings. The same conclusions drawn from plot 12 can be taken here. This parameter is indeed different for both particle species, confirming that $T_{\rm K}$ should not be used as a thermodynamical parameter for dense systems. As in the previous graph, $T_{\rm K}$ has two different regimes. One for high shear rate, where it scale with $\dot{\gamma}$ as a power law with exponent 1.26. The second one, where the jammed states are, this exponent is density dependent, the lowest being 0.61 and the highest 1.01.

All dashed lines and their respectively slopes are fits to the curve of $T_{\rm K}$ for the total number of particles, without any distinguishing from large or small. It should be noticed that the results of [28] indicate that the kinetic temperature is linearly dependent on the driving strength, the constant of proportionality being a function of the density and elasticity of the components of the mixture. Here we obtained a power law dependence between the two quantities. It should be noticed, however, that the previous results are for a granular bed, while ours is a 3D system. This difference may induce different dependencies in these parameters.

A comparison between Figures 12 and 13 with 8 and 9, respectively, implies that the effective temperature is always larger than the granular one in the jammed regime. We can also see that the behavior of $T_{\rm eff}$ with volume fraction is different from the behavior of $T_{\rm K}$ with ϕ. The last one decreases with increasing ϕ while the former increases. Also, one can clearly see that the ratio of the values of $T_{\rm K}$ for large and small particles is also constant, independent on the shear rate. This is the same observation that was made at the experiments of [28,29]. Their result, which was obtained for a system in a fluid-like state, also applies to a dense one, at least to the component T_{zz} of the temperature tensor (as defined in [30]). We did not studied the other components of this tensor. Finally, we see that the kinetic temperature is always larger for large grains, a result also observed in [28,29].

The growth of the exponent of $T_{\rm K}$ in $\dot{\gamma}$ with volume fraction can be seen in terms of the interaction between grains. Shearing a packing puts energy into it and the interactions dissipate this energy. As we lower the shear rate, enduring contacts build up as the main interaction mechanism. Since at lower volume fractions there are less contacts, diminishing $\dot{\gamma}$ does not cause a sharp drop on the average energy. For denser cases, the same reduction in shear rate causes the average energy to greatly lower its value due to the presence of more contacts. Therefore, $T_{\rm K}$ drops faster with increasing ϕ. Moreover,exponents are larger for friction packings due to the extra dissipation provided by tangential forces.

4 Calculation of the temperature via configurational averages

So far we have shown the existance of an effective temperature for jammed granular materials and argue that this could be a thermodynamical variable of the system because two different subsystems characterized by particles of different sizes have the same value of this parameter, as shown in Figure 10. This is a kind of zero-th law for the system. This property is not shared by, for instance, the granular temperature, and therefore it could not be thought of as a physical variable describing the thermodynamics of grains.

We also showed that the effective temperature is within the range of the temperature measured by other observables but only for the very long time behavior of the system, as shown in Figure 11. Thus our results suggest that this temperature may not capture all the thermodynamics of jamming.

Another test of the physical significance of $T_{\rm eff}$ is to compare its value with a temperature obtained directly by an average over the jammed configurations.

If it was true that a thermodynamic framework could describe the behavior of jammed systems, it stands to reason that the compactivity $X_{\rm E}$ of the granular packing given by equation (1) should be measured from a dynamical experiment involving the exploration of the jammed states. If the system is ergodic and amenable to a statistical mechanical approach, then the temperature defined by the configurational average should be the same as a dynamical measurement, as done for instance by the FDT.

To test this assumption is to test the ergodic hypothesis for jammed matter. Indeed, the statistical framework proposed by Edwards [3] is based on the fact that the jammed configurations are all equiprobable. This assumption is analogous to the basis under which the microcanonical ensemble of equilibrium statistical mechanics is built. However, this assumption has been very controversial for granular matter since grains are path dependent, frictional and non-conservative. In the absence of a Hamiltonian to describe the dynamics, there is no Liouville's theorem on which we can construct the statistical mechanics of grains from first principles. Thus, the idea of ergodicity for granular materials has received much opposition.

The validity of this statement was analyzed through computer simulations by Makse and Kurchan [5]. Our present results are an extension of these results. Here we reproduce the discussion of this paper to make an explicit connection with previous work. We will calculate the temperature from the entropy of the packing with a mathematical construction which assumes the jammed states to be equally probable. The temperature calculated from the entropy of the packing is compared to the effective temperature obtained dynamically. This is achieved via the procedure applied above which has for an aim to probe each static configuration by allowing the system to evolve at a very slow shear rate. This is done through the FDR which does not assume the flat average.

4.1 Exploring the jammed configurations via a flat average. Test of ergodicity: $T_{\rm eff} = X_{\rm E}$

The independent method to study the configurational space of grains allows us to investigate the statistical properties of the jammed states available at a given energy and volume. In turn, it is investigated whether it is possible to relate the dynamical temperature obtained above via a diffusion-mobility protocol to the configurational compactivity based on the flat average over jammed states.

In order to calculate $X_{\rm E}$ and compare with the obtained $T_{\rm eff}$, it is needed to sample the jammed configurations at a given energy and volume in an *equiprobable* way. In order to do this, the jammed configurations are sampled with the following probability distribution:

$$P_\nu \sim \exp[-E^\nu/T^* - E^\nu_{\rm jammed}/T_{\rm aux}]. \qquad (10)$$

Here the deformation energy E corresponds to the Hertzian energy of deformation of the grains. The extra term added in equation (10) allows the flat sampling of the jammed states to be perfomed. The jammed energy is such that it vanishes at the jammed configurations:

$$E_{\rm jammed} \propto \sum_i |\boldsymbol{F}_i|^2, \qquad (11)$$

where $\boldsymbol{F}_i$ is the total force exerted on a particle by its neighbors. The main property of this energy is that it should be zero at jamming.

Two "bath" temperatures are introduced (these temperatures are $\sim 10^{14}$ times the room temperature) which allow the exploration of the configuration space and the calculation of the entropy of the packing assuming a flat average over the jammed configurations. Equilibrium MD simulations are employed with two auxiliary "bath" temperatures $(T^*, T_{\rm aux})$, corresponding to the distribution (10). Annealing $T_{\rm aux}$ to zero selects the jammed configurations ($E_{\rm jammed} = 0$), while T^* fixes the energy E.

In practice, the equilibrium MD simulations are carried out with a modified potential energy:

$$U = \frac{T_{\rm aux}}{T^*} E + E_{\rm jammed}, \qquad (12)$$

and calculate the force on each particle from $\boldsymbol{F} = -\boldsymbol{\nabla} U$.

The auxiliary temperature $T_{\rm aux}$ is controlled by a thermostat which adjusts the velocities of the particles to a kinetic energy determined by $T_{\rm aux}$. We start by equilibrating the system at high temperatures ($T_{\rm aux}$ and $T^* \sim \infty$) and anneal slowly the value $T_{\rm aux}$ to zero and tune T^* so as to reach the value of E that corresponds to the average deformation energy obtained during shear.

The partition function is

$$Z = \sum_\nu \exp[-E^\nu/T^* - E^\nu_{\rm jammed}/T_{\rm aux}], \qquad (13)$$

from where the compactivity reads:

$$T^* = \frac{\partial E}{\partial S} \overset{T_{\rm aux} \to 0}{\longrightarrow} X_{\rm E}. \qquad (14)$$

Thus at the end of the annealing process ($T_{\rm aux} \to 0$), $T^*(E) = X_{\rm E}(E)$, since in this limit the sampled configurations have a vanishing number of moving particles at a given E.

Since a calculation of the force from a potential energy, equation (12), is required, only conservative systems can be studied with the method. Therefore it is not possible to test these ideas in a granular system with friction for it is a path-dependent system. Thus we focus our calculations on a system of frictionless particles.

A system of *frictionless* viscoelastic spherical particles could be thought of as a model of compressed emulsions [31,32], see also [33] for details. Even though they can be modeled in this way, an important difference arises in the inter-droplet forces, which are not given in terms of the bulk elasticity, as they are in the Hertz theory. Instead,

forces are given by the principles of interfacial mechanics [34]. For small deformations with respect to the droplet surface area, the energy of the applied stress is presumed to be stored in the deformation of the surface. The simplest approximation considers an energy of deformation which is quadratic in the area of deformation [34], analogous to a harmonic oscillator potential which describes a spring satisfying Hooke's law. More elaborated models have been proposed, and in a recent study the force law was calculated experimentally using confocal microscopic images of emulsions [16]. Here, we will avoid issues of path-dependency introduced by the interparticle tangential forces, by excluding these forces from the calculation ($F_{\rm t} = 0$). Because there are no transverse forces, the grains slip without resistance and this procedure essentially mimics the path to jammed states for the compressed emulsion system.

Thus, the MD model of granular materials is adapted to describe the system of compressed emulsions by only excluding the transversal forces (tangential elasticity and Coulomb friction). The continuous liquid phase is modeled in its simplest form, as a viscous drag force acting on every droplet, proportional to its velocity. The systems under investigation have exponentially large (in the number of particles) number of stable states jammed at zero bath temperature. Thus, a meaningful annealing procedure is only possible for very small system sizes with the present computational power. Therefore, the system of study has 200 particles only.

The calculations for the effective temperature for this system have been done in [5]. The effective temperature is $T_{\rm eff} = 2.8 \times 10^{-5}$, the mean pressure $P = 10$ MPa, the volume fraction $\phi = 0.66$ and the mean compressional energy $\langle E \rangle = 8.4 \times 10^{-4}$ J. All these values have been obtained during the shear of the material.

In the calculation of the compactivity for the same system of 200 frictionless particles at the same pressure and volume fraction, there is no dynamics so the viscous forces of dissipation are completely disregarded. At the end of the annealing protocol the compactivity at a given deformation energy can be obtained as illustrated in Figure 14.

In the begining, the system is equilibrated for 40×10^6 iterations at high auxiliary temperatures, such as at point A in Figure 14: ($T^* = 3.4 \times 10^{-2}, T_{\rm aux} = 3 \times 10^{-8}$). Different annealing paths are taken for T^*, one decreases its value to $T^* = 2.9 \times 10^{-4}$ (open squares, path 1a) and the other anneals it to $T^* = 3.4 \times 10^{-3}$ (filled circles, path 1). Path 1a is followed until the value of T^* reaches 2.9×10^{-5}. Path 1 continues until both temperatures are annealed to the point where this path is split again: one branch anneals T^* to 2.9×10^{-5} (open diamonds, path 1b), joining the line of path 1a, while the other anneals to $T^* = 3.4 \times 10^{-4}$. From this point on, T^* is kept constant in paths 1a and 1b, while annealing $T_{\rm aux}$ to zero. Path 1 continues until it reaches point B, with $T_{\rm aux} = 3 \times 10^{-10}$), where it is split for the last time in three different branches: one keeps T^* constant at 3.4×10^{-4} (filled right triangles, path 3), the second

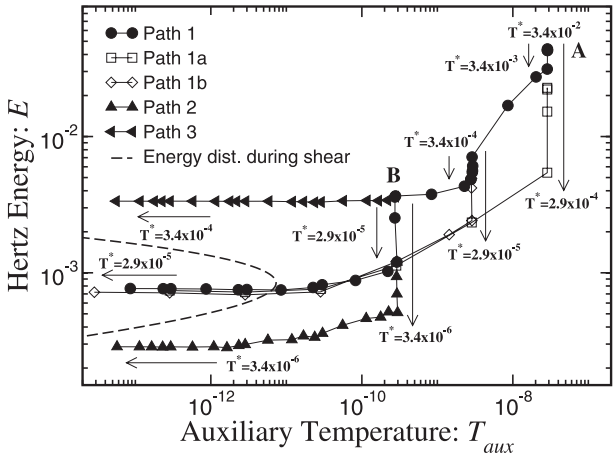

Fig. 14. Annealing procedure to calculate $X_{\rm E}$ at different elastic compressional energies. We plot the elastic energy *vs.* $T_{\rm aux}$ during annealing together with the distribution of elastic energies obtained during shear (dashed curve, mean value $\langle E \rangle = 8.4 \times 10^{-4}$). At the end of the annealing we find that the energy is very similar to the average energy for the sheared system only when we set $T^* = X_{\rm E}$.

anneals T^* to the value 2.9×10^{-5}, the last one anneals T^* to 3.4×10^{-6} (filled triangles, path 2). When $T^* = T_{\rm eff}$ (Paths 1, 1a and 1b), the final elastic compressional energy value when $T_{\rm aux} \to 0$ falls inside the distribution of energies obtained, and it is very close to the mean value of the elastic energy during shear $\langle E \rangle$. The remarkably result is that this implies that the compactivity and the effective temperature obtained dynamically are found to coincide to within computational error,

$$X_{\rm E} \approx T_{\rm eff}. \tag{15}$$

For other values of $T^* \neq T_{\rm eff}$ the final E falls out of the distribution obtained during shear (Paths 2 and 3).

This provides evidence for the validity of the effective temperature as a dynamical estimate of the compactivity, and more importantly, justifies the use of the statistical measurements presented in characterizing the macroscopic properties of the jammed system. Since $T_{\rm eff}$ does not assume the flatness of the jammed states because it is obtained dynamically, these results indicate that, at least in the present system, the ergodic hypothesis for granular matter is a plausible approximation to the dynamics of the system.

The conclusion is that the jammed configurations explored during shear are sampled in an equiprobable way as required by the ergodic principle. Moreover, the dynamical measurement of compactivity renders the thermodynamic approach amenable to experimental investigations [13].

It should be noted though that this is only an approximation, and it is valid only when the granular material is pretreated so that it is in a reversible state. In computer simulations, the reversible state is achieved by simulating packings without friction as explained before. In the case of friction, it is still possible to generate packings which are reversible and amenable to a statistical

description. This problem has been treated before in [16,35]. Experimentally, it has been also shown that granular matter should show reversibility if it is properly prepared, even when system has friction and path-dependent forces. The seminal experiments of the Chicago group of column tapping [36,37] clearly indicate the existance of these reversible jammed states in granular materials. Moreover these experiments have been reproduced by other groups as well [38] and under other conditions such as oscillatory pressure [39]. These reversible states are the ones for which the statistical mechanics is possible. Notice that this assumption preclude other simple systems such as a pile of grains. A sandpile, for instance, is not in a reversible state since any perturbation will deform the pile. Moreover, there is a whole branch of irreversible states that have been obtained in the Chicago experiments and in the experiments of Brujic *et al.* [39], before the reversibility is achieved.

The present thermodynamics is not applied to such systems. Other theories, such as the fragile matter theory of Cates *et al.* [46] might be able to capture this irreversible states of granular matter.

5 System properties

In this section, we investigate how other properties of our system behave as a function of the shear rate and density. The properties observed were the average potential energy, pressure, and shear stress during shear (only shear stress from now on) and apparent shear viscosity. We want to know how jamming affects these properties. We only show results for the shear stress and the viscosity, since the potential energy and pressure behave qualitatively as the shear stress. All the properties are calculated when the system enters the steady state. Therefore, they are given as simple time averages.

5.1 Shear stress

The shear stress is defined as the xy-component of the stress tensor σ_{ij}. In fact, we measured the shear stress which arises from compression and do not include the contribution from momentum exchange between grains. In complex fluids, the average shear stress is usually fitted to a power law, the Herschel-Bulkeley equation [40]:

$$\langle\sigma_{xy}\rangle = \sigma_0 + A\dot{\gamma}^n, \tag{16}$$

where σ_0 is the yield stress and A is a constant [19,41,42].

In Figure 15 is shown the results for $\langle\sigma_{xy}\rangle$ for the frictionless case. It is observed a plateau at higher volume fractions and small shear rates. The plateaus correspond to the yield stress σ_0 in equation (16). It is not surprising to observe a non-vanishing yield stress since equilibration of such packings implies that. What is interesting is the absence of an yield stress for the $\phi = 0.6428$ state, initially in the solid-like state. This confirms that this system is unstable under shear and it is not truly jammed. Also, we let the system relax after shearing and observe that, indeed, $\langle\sigma_{xy}\rangle \to 0$. The existence of a yield stress can be considered as an instance of the jamming transition [19,41–44].

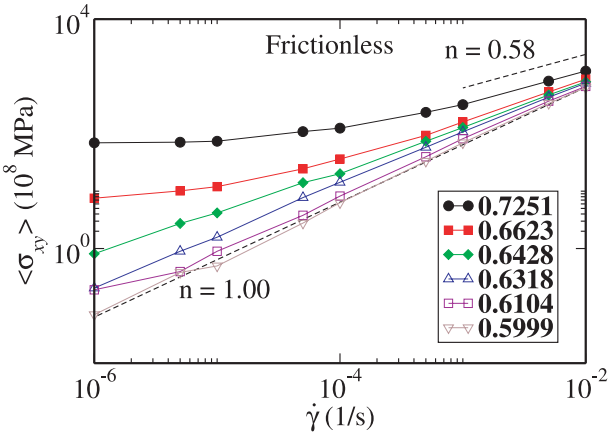

Fig. 15. Average shear stress *vs.* shear rate, no friction. The plateaus are the evidence of a jamming transition. The dashed lines are explained in the text. The numbers are their slopes.

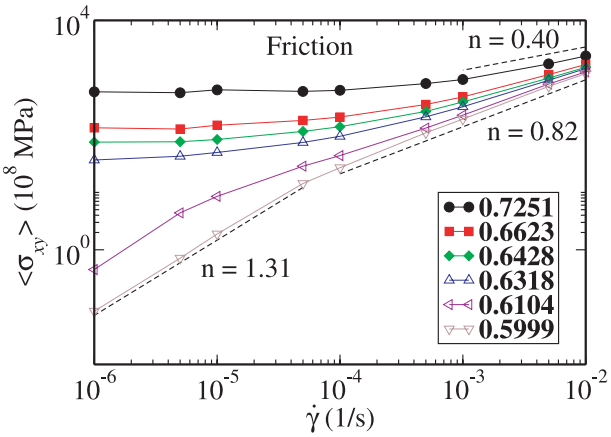

Fig. 16. Average shear stress *vs.* shear sate, friction. As in Figure 15 the plateaus correspond to jammed states. Dashed lines, showed with the correspondent slopes, are explained in the text.

As we go up in shear rate, the stress increases as a power law whose exponent depends on the volume fraction (in the cases of the thermal systems, this exponent depends on the bath temperature [41,42]). The upper dashed line in 15 is a fit to the last 3 points in the flow curve for the $\phi = 0.7251$ case. The lower curves do not display a yield stress, but they match the opposite limit of the phenomenology of the shear stress, the power-law-fluid regime [19,41,42]. The lower dashed line is a fit to the flow curve of the $\phi = 0.5999$ state, showing that this state corresponds to a Newtonian fluid. The two middle curves match the behavior of power-law fluid, with the exponent n of equation (16) density dependent.

In Figure 16 we have the frictional results for $\langle\sigma_{xy}\rangle$. We notice that there are four states that develop an yield stress, the same four that display a plateau in the effective temperature results. As in the frictionless case, at high shear rate the main contribution to the shear stress is the

second term on right hand side of equation (16). Again the exponent n depends on volume fraction. Its lowest value comes from the slope of the 3 last points in the $\langle\sigma_{xy}\rangle$ curve for the $\phi = 0.7251$. On the other hand, it seems that, at lower volume fractions, the systems displays two different regimes, without an yield stress, in conflict with what is expected from the Herschel-Bulkeley equation. These two regimes are exemplified by the two lower dashed lines which are fits to the first 4 points and to the last 5 points in the $\phi = 0.5999$ flow curve. We would expect this curve to have a unity slope and this to be the Newtonian regime This fact deserves more investigation, since friction is inherent to grains, and its presence could alter significantly the behavior of the shear stress at low shear rate. The important conclusion is that at high shear rate the exponent n is still density dependent and increases with smaller density, eventually reaching 1. Moreover, we also expect that at higher shear rates, the average shear stress should scale as $\langle\sigma_{xy}\rangle \sim \dot{\gamma}^2$, the well-known Bagnold scaling [45].

By looking at the results for $T_{\rm eff}$, the plots for shear stress confirm the two conclusion drawn before: instability of frictionless systems at densities up to $\phi = 0.64$, at least (this is evidence of the fragility concept proposed to describe granular matter by Cates *et al.* [46]) and the shear-induced jamming transition. We can see that the plateaus in the shear stress (the yield stress), in the frictionless and frictional cases, correspond to the plateaus in the plots for $T_{\rm eff}$. Therefore, these states are the jammed states of our system. In this way, we can say that the appearance of a well-defined effective temperature is a consequence of the development of an yield stress [10,19,43,44].

The packing instability can be explained by the fact that when shear is stopped, the grains become less compressed by pushing one another in order to attain a minimum of potential energy. While they push each other, they also slide related to their neighbors, breaking the contacts. When all, or most, of these contacts are broken all quantities that depend on the overlap between grains (potential energy, pressure, shear stress), should drop to zero, since the amount of compression is negligible. This relaxation does not happen at higher ϕ because there is no available space for the grains to fully relax.

In the friction packings, the same mechanism of relaxation is present. This difference in the flow curves is a consequence of the fact that the remaining normal forces, responsible for separating the particles, are not strong enough to break the contacts, which are supported by the tangential forces. Therefore, we say that our system undergoes a shear-induced jamming transition in the case $\phi = 0.6318$. The shear induces contacts between particles and these shear-induced contacts survive after the shear is stopped, providing the system an yield stress.

5.2 Apparent shear viscosity

The last of the macroscopic observables probed is the apparent shear viscosity of the system, η, defined as:

$$\eta = \frac{\langle\sigma_{xy}\rangle}{\dot{\gamma}}. \tag{17}$$

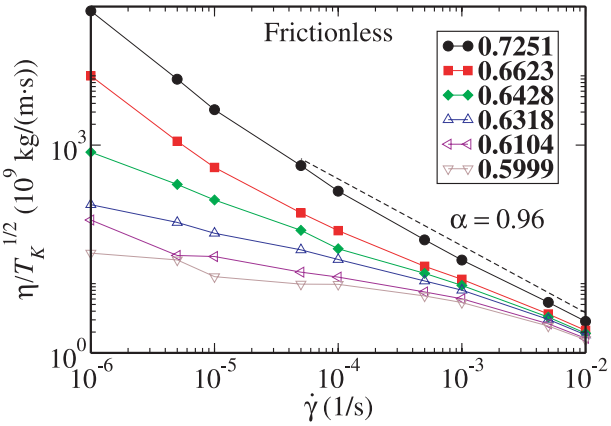

Fig. 17. η normalized by ${T_{\rm K}}^{1/2}$, frictionless case. The slope of the dashed line indicate the regime we can find the system.

Using equation (16), we can rewrite this expression as [19]:

$$\eta = A\dot{\gamma}^{-\alpha(\phi)}. \tag{18}$$

From this equation we can see that, according to the value of n, the system may display three different regimes: shear-thinning ($\alpha(\phi) > 0$), Newtonian ($\alpha(\phi) = 0$) or shear-thickening ($\alpha(\phi) < 0$). Measurements of viscosity have been performed in a variety of complex fluids, for example glasses [20,19], foams [41,42], and colloids [23,47–49]. In some of these systems, a shear-thinning behavior, with exponents between 0.6 and 1.0, was observed [19,20,49], and in others both shear-thinning and shear-thickening are present [47,48].

The calculation of equation (17) is not as direct as it seems. First of all it should be noticed that in the fluid state the viscosity scales as $T_{\rm K}^{1/2}$ [30,50]. The reason behind this dependence is that in these cases, the grain movement is a consequence of the application of shear, which inputs energy in the system. This energy input, for instance, increases the kinetic energy of the grains. Therefore, the shear rate and the kinetic temperature (9) are coupled. Since this input in energy leads to higher $T_{\rm K}$, more collision take place and, consequently, the system reaches a higher stress. We should, then, plot the viscosity normalized by $T_{\rm K}^{1/2}$ in order to disregard this effect on η.

In Figure 17 we plot $\eta/T_{\rm K}^{1/2}$ for frictionless packings. We see that at low shear rate and low volume fractions we have approximately Newtonian behavior, already expected by the result from the shear stress, Figure 15. This is the effect of the high velocities imposed on the system at this regime. Particles move so fast that they do not seem to "see" each other and then the whole viscosity drops. At higher volume fractions we clearly observe a shear-thinning behavior. We show a fit to the last 5 points for the $\phi = 0.7251$ curve. The slope is inside the range reported for many soft materials [19,20,49].

These regimes are more clearly observed in the friction case, Figure 18. At lower densities and smaller shear rates, we have a Newtonian behavior with α close to zero. The situation is a bit different at higher densities and low shear

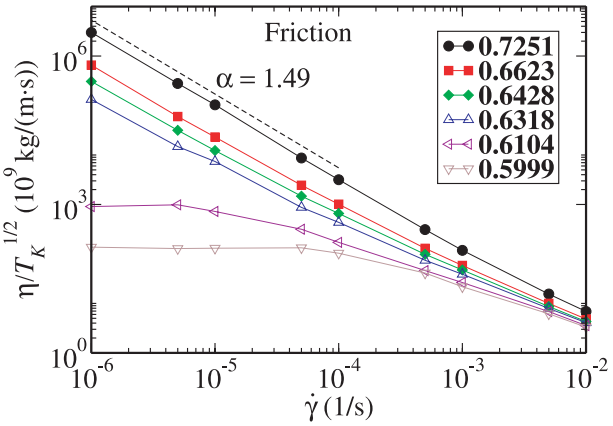

Fig. 18. η normalized by ${T_\mathrm{K}}^{1/2}$, friction case. The Newtonian regime is clearer here. The dashed line is explained in the text.

rates. The slope of the fit (dashed line) for the first 5 points in the $\phi = 0.7251$ curve is outside the known range for complex fluids. Again, friction may be playing a major role and more investigation is needed to elucidate this matter. It is important to check the behavior in the fluid regime, states with $\phi = 0.5999$, 0.6104 and 0.6318. In the first two of them, we have a Newtonian behavior as expected for $\eta/T_\mathrm{K}^{1/2}$. The third one displays shear-thinning since it is jammed, see Figures 15 and 16. The results for the other states should be taken carefully, especially regarding the values of the exponents α. But the trend is correct, the system should display shear-thinning at high shear rate as a result of jamming.

6 Conclusions

In this paper we study the effective temperature of sheared, bi-disperse, dense granular system in three dimensions as a function of the shear rate and volume fraction. We consider systems in which grains interact by purely repulsive forces, frictionless case, and others that they interact by normal and tangential forces, friction case.

The effective temperature (2) is shown to be independent on the shear rate at volume fractions of the order, and above, of $\phi = 0.68$ for the frictionless case, and $\phi = 0.63$ for the friction case. This effective temperature is shown to be equal to both large and small particles, indicating that such parameter is at least consistent with a zero-th law of thermodynamics for grains. It is shown that T_eff has some dependence on the observable as we had only approximate agreement with a temperature measured from the ISF. However, we present enough evidence pointing toward the fact that the effective temperature is an intrinsic property of the system and, along with experimental results [13], that a thermodynamics of granular materials is feasible.

The fact that slow relaxation modes can be characterized by a temperature raises the question of the existence of a form of ergodicity for the structural motion, allowing a construction of a statistical mechanics ensemble for the slow motion of the grains. This argument leads us back to the ideas of the thermodynamics of jammed states. In parallel to these dynamical measurements, the same information is drawn from the system by a flat statistical average over the jammed configurations. Once all the static configurations have been visited by the system, the compactivity X_E can be calculated from the statistics of the canonical ensemble of the jammed states. The logarithm of the available configurations at a given energy and volume reveals the entropy, from which the compactivity is calculated. Our explicit computation shows that the temperature arising from the Einstein relation (2) can be understood in terms of the configurational compactivity X_E arising from the statistical ensemble of jammed states.

We also investigate the role played by the kinetic energy in the system. The granular temperature does not share the properties of T_eff. It has a power-law dependence on the shear rate with exponents that increase with volume fraction. This is a direct consequence of the enduring contacts between grains.

The jamming transition is observed in the behavior of other observable we studied, namely shear stress and apparent shear viscosity. The states with volume fractions higher than $\phi = 0.68$ and $\phi = 0.63$ in the frictionless and friction cases develop a yield stress. This is clear indication that the system jammed. Moreover, we showed that our system obeys the Herschel-Bulkeley law (16). We observed that the exponent is density dependent (in analogy with other soft materials, where it is proportional to the external bath temperature). This parameter tends, at high shear rate and low volume fraction, to 1, in the frictionless case, where the system behaves like a power-law fluid [19]. We did not observe this in the friction case. In fact at lowest volume fraction, the system displays two different exponents, and no yield stress. We attribute this to the possibility that friction between particle could invalidate (16) for grains in some range of ϕ.

The apparent viscosity, normalized by the square root of the granular temperature, displays the predicted behavior of shear-thinning observed for others complex fluids at high volume fractions [19,20,30,49]. It depends as a power law on $\dot{\gamma}$ with an exponent which depends on the volume fraction, and approaches -1.0 as ϕ increases in the frictionless case. This exponent is characteristic of complex fluids in jammed states. The system shows a Newtonian behavior at low volume fraction and shear rate. In the friction case, the Newtonian behavior is even clearer, but we measured an exponent in equation (18) which is outside the known range for complex fluids, and this may be, again, the presence of friction. However, the trends we obtained are important. We observe a shear-thinning behavior for the system as long as it stays jammed. All these results led to the conclusion that by applying shear to a granular packing we can induce a jamming transition (observed for the friction case at volume fraction of $\phi = 0.6318$) or we can unjam a system (observed for the frictionless case at volume fraction of $\phi = 0.6428$).

We thank Mark Shattuck for many valuable discussions. This work is supported by the National Science Foundation, the Department of Energy and CAPES (Brazilian agency).

References

1. R.G. Larson, *The structure and rheology of complex fluids* (Oxford University Press, New York, 1998)
2. H.M. Jaeger, S.R. Nagel, R.P. Behringer, Rev. Mod. Phys. **68**, 1259 (1996)
3. S.F. Edwards, R.S.B. Oakeshott, Phys. A **157**, 1080 (1989)
4. H.A. Makse, J. Brujić, S.F. Edwards, in *The Physics of Granular Media*, edited by H. Hinrichsen, D.E. Wolf (Wiley-VCH Verlag, 2004)
5. H.A. Makse, J. Kurchan, Nature **415**, 614 (2002)
6. L.F. Cugliandolo, J. Kurchan, L. Peliti, Phys. Rev. E **55**, 3898 (1997)
7. G. Parisi, Phys. Rev. Lett. **79**, 3660 (1997)
8. J.-L. Barrat, W. Kob, Europhys. Lett. **46**, 637 (1999)
9. F. Sciortino, P. Tartaglia, Phys. Rev. Lett. **86**, 107 (2001)
10. L. Berthier, J.-L. Barrat, Phys. Rev. Lett. **89**, 95702 (2002)
11. M. Nicodemi, Phys. Rev. Lett. **82**, 3734 (1999)
12. I.K. Ono, C.S. O'Hern, D.J. Durian, S.A. Langer, A.J. Liu, S.R. Nagel, Phys. Rev. Lett. **89**, 95703 (2002)
13. C.M. Song, P. Wang, H.A. Makse, Proc. Nat. Acad. Sci. **102**, (2005) 2299
14. P.A. Cundall, O.D.L. Strack, Géotechnique **29**, (1979) 47
15. K.L. Johnson, *Contact Mechanics* (Cambridge University Press, Cambridge, 1985)
16. H.P. Zhang, H.A. Makse, Phys. Rev. E **72**, 11301 (2005)
17. H.A. Makse, D.L. Johnson, L.M. Schwartz, Phys. Rev. Lett. **84**, 4160 (2000)
18. M.P. Allen, D.J. Tildesley, *Computer simulation of liquids* (Oxford University Press, New York, 1996)
19. L. Berthier, J.-L. Barrat, J. Chem. Phys. **116**, 6228 (2002)
20. R. Yamamoto, A. Onuki, Phys. Rev. E **58**, 3515 (1998)
21. G. D'Anna, G. Gremaud, Nature **413**, 407 (2001)
22. R.S. Farr, J.R. Melrose, R.C. Ball, Phys. Rev. E **55**, 7203 (1997)
23. E. Bertrand, J. Bibette, V. Schmitt, Phys. Rev. E **66**, 60401 (2002)
24. J.-P. Hansen, I.R. McDonald, *Theory of simple liquids* (Academic Press, San Diego, 2003)
25. S. Sastry, P.G. Debenedetti, F.S. Stillinger, Nature **393**, 554 (1998)
26. W. Kob, H.C. Andersen, Phys. Rev. E **52**, 4134 (1995)
27. K. Miayazaki, D.R. Reichman, R. Yamamoto, e-print `arXiv:cond-mat/0401528` (2004)
28. K. Feitosa, N. Menon, Phys. Rev. Lett. **88**, 198301 (2002)
29. R.D. Wildman, D.J. Parker, Phys. Rev. Lett. **88**, 64301 (2002)
30. C. Bizon, M.D. Shattuck, J.B. Swift, H.L. Swinney, Phys. Rev. E **60**, 4340 (1999)
31. M.-D. Lacasse, G.S. Grest, D. Levine, T.G. Mason, D.A. Weitz, Phys. Rev. Lett. **76**, 3448 (1996)
32. D.J. Durian, Phys. Rev. Lett. **75**, 4780 (1995)
33. J. Brujić, S.F. Edwards, D.V. Grinev, I. Hopkinson, D. Brujić, H.A. Makse, Faraday Discuss. **123**, 207 (2003)
34. H.M. Princen, J. Colloid Interface Sci. **91**, 160 (1983)
35. H. A. Makse, N. Gland, D.L. Johnson, L. Schwartz, Phys. Rev. E **70**, 061302 (2004)
36. E.R. Nowak, J.B. Knight, M.L. Povinelli, H.M. Jaeger, S.R. Nagel, Powder Technol. **94**, 79 (1997)
37. E.R. Nowak, J.B. Knight, E. Ben-Naim, H.M. Jaeger, S.R. Nagel, Phys. Rev. E **57**, 1971 (1998)
38. P. Philipe, D. Bideau, Europhys. Lett. **60**, 677 (2002)
39. J. Brujić, P. Wang, C. Song, D.L. Johnson, O. Sindt, H.A. Makse, Phys. Rev. Lett. **95**, 128001 (2005)
40. S.D. Holdsworth, Trans. Inst. Chem. Eng. **71**, 139 (1993)
41. P. Sollich, F. Lequeux, P. Hébraud, M.E. Cates, Phys. Rev. Lett. **78**, 2020 (1997)
42. P. Sollich, Phys. Rev. E **58**, 738 (1998)
43. M. Matsuo, e-print `arXiv:cond-mat/0108268` (2001)
44. C.S. O'Hern, L.E. Silbert, A.J. Liu, S.R. Nagel, Phys. Rev. E **68**, 11306 (2003)
45. R.A. Bagnold, Proc. R. Soc. London Ser. A **225**, 49 (1954)
46. M.E. Cates, J.P. Wittmer, J.-P. Bouchaud, P. Claudin, Phys. Rev. Lett. **81**, 1841 (1998)
47. V. Trappe, V. Prasad, L. Cipelletti, P.N. Segre, D.A. Weitz, Nature **411**, 772 (2001)
48. Y.S. Lee, N.J. Wagner, Rheol. Acta **42**, 199 (2003)
49. D. Bonn, S. Tanase, B. Abou, H. Tanaka, J. Meunier, Phys. Rev. Lett. **89**, 15701 (2002)
50. L. Bocquet, W. Losert, D. Schalk, T.C. Lubensky, J.P. Gollub, Phys. Rev. E **65**, 11307 (2001)